

Doping evolution of the normal state magnetic excitations in pressurized $\text{La}_3\text{Ni}_2\text{O}_7$

Hai-Yang Zhang, Yu-Jie Bai, Fan-Jie Kong, Xiu-Qiang Wu, Yu-Heng Xing, and Ning Xu
Department of Physics, Yancheng Institute of Technology, Yancheng 224051, China

(Dated: December 30, 2024)

The doping evolution behaviors of the normal state magnetic excitations (MEs) of the nickelate $\text{La}_3\text{Ni}_2\text{O}_7$ are theoretically studied in this paper. For a filling of $n = 3.0$ which corresponds roughly to the material which realizes the superconductivity of about 80 K under moderately high pressures above 14 GPa, the MEs exhibit a square-like pattern centered at $(0,0)$ which originates from the intrapocket particle-hole scatterings. Furthermore, it was found that the MEs show very strong modulations on the interlayer momentum q_z . With the increasing of q_z , the patterns of the MEs change dramatically. In the large q_z regime, they turn to be ruled by the interpocket excitation modes with significantly larger intensity which may play a vital role in the superconducting pairing. This hidden feature of the MEs was not revealed by previous studies. The established features of the MEs are found to be very robust against doping. They persist in the wide hole- or electron-doping regime around $n = 3.0$. However, in the heavily electron-doped regime, a Lifshitz transition will occur. Consequently, the behaviors of the MEs change qualitatively across this transition. With the absence of the hole pocket, we predict that a strong tendency toward the spin-density-wave (SDW) order will develop due to the perfect nesting between the electron and the hole pockets at $n = 4.0$. Thus, we have investigated the normal state behaviors of the MEs and their doping evolutions which may shed light on the mechanism of superconductivity in pressurized $\text{La}_3\text{Ni}_2\text{O}_7$.

I. THE INTRODUCTION

The newly discovered superconductivity with a transition temperature above 80 K in the moderately pressurized $\text{La}_3\text{Ni}_2\text{O}_7$ has attracted much attention in condensed matter community [1]. Zero resistance was achieved in single [2–5] and polycrystalline [6] samples by using the liquid pressure medium. It was found that, generally, the emergence of superconductivity is accompanied by the lattice structure transition driven by the applied pressure [2, 5]. According to a recent report, the superconductivity persists up to 90 GPa with a right-triangle shaped phase region [5]. Although intensive studies have been carried out, the mechanism of superconductivity is still a hotly debated issue [7–32]. The density functional theory (DFT) calculations reveal that the low energy electronic bands of $\text{La}_3\text{Ni}_2\text{O}_7$ are ruled by the Ni- $3d_{z^2}$ and Ni- $3d_{x^2-y^2}$ orbitals and the superconductivity shows up with the presence of a hole pocket mainly of the Ni- $3d_{z^2}$ orbital character around the Fermi level [2]. Both the band structure and the topology of the Fermi surfaces obtained by DFT are recently confirmed by the ARPES measurements at ambient pressure [33, 34]. Due to the strong hybridization between the Ni- $3d_{z^2}$ orbital and the apical O- p_z orbital, the interlayer antiferromagnetic coupling of the $3d_{z^2}$ orbitals was proposed to be important [18, 22, 31]. So far, there have been accumulated evidences that a SDW order may develop around 150 K in the parental compounds [35–38]. In this way, the external pressure seems to play the similar role of charge carrier doping in cuprates to suppress the magnetic order and give birth to superconductivity. This proximity of the magnetic phase to superconductivity resembles that of many other unconventional superconductors, such as copper oxides [39, 40] and iron-based pnictides [41]. As well known, it was believed that the magnetic fluctuations play a vital role in pairing of these materials [41]. To date, several candidates for the mechanism of superconductivity in pressurized $\text{La}_3\text{Ni}_2\text{O}_7$ had been theoretically proposed based on the magnetic-mediated inter-

action scenarios [9, 14, 22, 23, 26, 28]. However, the origin of superconductivity is still unsettled. Thus, the investigation of the normal state MEs is highly desired as it may reveal the intimate relation between magnetic fluctuations and superconductivity in pressurized $\text{La}_3\text{Ni}_2\text{O}_7$.

In this paper, adopting the previously proposed bilayer-two-orbital model of Ref. [7], we theoretically studied the normal state behaviors of the MEs in the nickelate $\text{La}_3\text{Ni}_2\text{O}_7$. As indicated by the DFT calculations, the band structures of $\text{La}_3\text{Ni}_2\text{O}_7$ exhibit remarkable dependence on pressure. The hole pocket is slightly below the Fermi level at ambient pressure, however, it approaches and finally intersects with the Fermi level in the high pressure regime [1]. That is, the Lifshitz transition will develop, driven by the applied pressure. Besides this, it is unclear how pressure affects the electronic energy bands in details. Here, the doping evolution behaviors of the MEs were studied for the pressurized $\text{La}_3\text{Ni}_2\text{O}_7$. We hope some of the results may be applied to this material. Firstly, we focus on the case with a filling number of $n = 3.0$ which corresponds roughly to the material which realizes the superconductivity of about 80 K under a pressure of about 14 GPa [1]. It was found that the behaviors of the MEs have very strong dependence on the vertical momentum q_z associated with the displacement between the upper and the lower nickel-oxygen layers. With q_z near zero for which the interlayer spins align parallelly, the MEs exhibit a square-like pattern centered at $(0,0)$ which originates mainly from the intrapocket particle-hole scatterings of the β band. With the gradually increasing of q_z , the MEs change dramatically. Specifically, for large q_z near π , they turn to be dominated by two kinds of modes associated with the interpocket particle-hole scatterings. One of which originates from the particle-hole scatterings between the α and the β pockets. While the other arises from the scatterings between the β and the γ pockets. These two modes have larger intensity compared to those with small q_z . Thus, they are expected to play more prominent roles if the pairing of electrons is mediated by magnetic fluctuations.

Secondly, we find that these features of the MEs are very robust in the wide doping region around $n = 3.0$. The patterns of the MEs and their energy and q_z dependence keep qualitatively unchanged regardless of whether the system is hole- or electron-doped. Finally, for the heavily electron-doped system, a Lifshitz transition will occur. We find that the behaviors of the MEs will change qualitatively across this transition. When the hole γ pocket is absent, a strong tendency toward the SDW order develops due to the well-nesting behavior between the α and the β pockets. Thus, we have studied extensively the normal state behaviors of the MEs across a wide doping regime, which may shed light on the mechanism of superconductivity in pressurized $\text{La}_3\text{Ni}_2\text{O}_7$.

II. THE MODEL AND FORMULAS

We adopt the bilayer-two-orbital Hamiltonian $H = H_0 + H_I$ to carry out the calculations, where the tight-binding part of the Hamiltonian reads $H_0 = \sum_{kab\sigma}^{LJ} \varepsilon_{ab}^{LJ}(k) C_{La\sigma}^+(k) C_{Jb\sigma}(k)$ [7] with L, J the layer indices, while a, b and σ the orbital and spin indices, respectively. The kinetic energy terms are $\varepsilon_{xx/zz}^{LL}(k) = -2t_1^{x/z} \gamma_k - 4t_2^{x/z} \gamma_k' + \varepsilon^{x/z} - \mu$, $\varepsilon_{xz}^{LL}(k) = 2t_3^{xz} \gamma_k''$, $\varepsilon_{xx/zz}^{LL}(k) = 2t_{\perp}^{x/z}$, $\varepsilon_{xz}^{LL}(k) = 2t_4^{xz} \gamma_k''$, with $\gamma_k = \cos k_x + \cos k_y$, $\gamma_k' = \cos k_x \cos k_y$ and $\gamma_k'' = \cos k_x - \cos k_y$, while x and z denote the $\text{Ni-}3d_{x^2-y^2}$ and $\text{Ni-}3d_{z^2}$ orbital, respectively. The hopping integrals are $t_1^x = -0.483$, $t_1^z = -0.110$, $t_2^x = 0.069$, $t_2^z = -0.017$, $t_3^{xz} = 0.239$, $t_{\perp}^x = 0.005$, $t_{\perp}^z = -0.635$, $t_4^{xz} = -0.034$, $\varepsilon^x = 0.776$ and $\varepsilon^z = 0.409$ as listed in Ref [7].

The interacting part of the Hamiltonian H_I is given by,

$$\begin{aligned} H_I = & U \sum_{L,i,a} n_{Lia\uparrow} n_{Lia\downarrow} + U' \sum_{L,i,a<b} n_{Lia} n_{Lib} \\ & + J \sum_{L,i,a<b} C_{Lia\sigma}^+ C_{Lib\sigma'}^+ C_{Lia\sigma'} C_{Lib\sigma} \\ & + J' \sum_{L,i,a\neq b} C_{Lia\uparrow}^+ C_{Lia\downarrow}^+ C_{Lib\downarrow} C_{Lib\uparrow}. \end{aligned} \quad (1)$$

Where $n_{Lia} = n_{Lia\uparrow} + n_{Lia\downarrow}$ is the occupation number of the orbital a electron at site i of layer L . U, U', J, J' are the coefficients of the intraorbital interaction, interorbital interaction, Hund coupling and pair hopping terms, respectively. The constrains $U = U' + J + J'$ and $J = J'$ are used throughout the paper as required by the spatial and spin rotational symmetry.

We study the normal state MEs of $\text{La}_3\text{Ni}_2\text{O}_7$ within the RPA approximation which had been used to study the MEs of various unconventional superconductors [42–55]. It had been justified by these studies that the main features of the MEs can be qualitatively captured by this method. In the present model, the single particle Green's function can be defined as $\hat{G}_{ab\sigma}^{LJ}(k, \tau) = -\langle T[C_{La\sigma}(k, \tau) C_{Jb\sigma}^+(k, 0)] \rangle$. Due to the spin $SU(2)$ symmetry of the model, we restricted ourself to the transverse spin susceptibility which is defined as $\hat{\chi}_{ab,cd}^{LJ, KM}(q, \tau) = \langle T[S_{La,Jb}^-(q, \tau) S_{Kc, Md}^+(q, 0)] \rangle$, where $S_{La,Jb}^-(q) = \frac{1}{\sqrt{N}} \sum_k C_{La\downarrow}^+(k) C_{Jb\uparrow}(k+q)$ and $S_{La,Jb}^+(q) = \frac{1}{\sqrt{N}} \sum_k C_{La\uparrow}^+(k+q) C_{Jb\downarrow}(k)$ are the spin lowering and ris-

ing operators, respectively, with N the number of the lattice sites. The bare spin susceptibility can be expressed as $\hat{\chi}_{ab,cd}^{LJ, KM}(q, \tau) = -\frac{1}{N} \sum_k G_{da\downarrow}^{ML}(k, -\tau) G_{bc\uparrow}^{JK}(k+q, \tau)$. After the fourier transformation, we get $\hat{\chi}_{ab,cd}^{LJ, KM}(q, i\omega_n) = -\frac{1}{N\beta} \sum_{k, i\omega_m} G_{da\downarrow}^{ML}(k, i\omega_m) G_{bc\uparrow}^{JK}(k+q, i\omega_m + i\omega_n)$, where $\beta = \frac{1}{T}$ is the inverse of the temperature T .

Decomposed into the spin channel, the nonzero elements of the interaction matrix read as $\hat{U}_{aa,aa}^{LL,LL}(q) = U$, $\hat{U}_{aa,bb(a\neq b)}^{LL,LL}(q) = J$, $\hat{U}_{ab,ba(a\neq b)}^{LL,LL}(q) = U'$ and $\hat{U}_{ab,ab(a\neq b)}^{LL,LL}(q) = J'$. In this way, the RPA spin susceptibility can be written as $\hat{\mathcal{X}}(q, i\omega_n) = \hat{\chi}(q, i\omega_n) (\hat{I} - \hat{U}(q) \hat{\chi}(q, i\omega_n))^{-1}$. After the analytic continuation, the retarded spin susceptibility $\hat{\mathcal{X}}^R(q, \omega) = \hat{\mathcal{X}}(q, \omega + i\Gamma)$ can be obtained, where Γ is the broadening factor which is set to be 0.02 in this paper. Actually, for the double-layer system $\text{La}_3\text{Ni}_2\text{O}_7$, the imaginary part of the spin susceptibility can be decomposed into the intralayer and interlayer components as $\mathcal{X}_S''(q, \omega) = \sum_{Lab} \text{Im}(\hat{\mathcal{X}}^R)_{aa,bb}^{LL,LL}(q, \omega)$ and $\mathcal{X}_D''(q, \omega) = \sum_{Lab} \text{Im}(\hat{\mathcal{X}}^R)_{aa,bb}^{LL,LL}(q, \omega)$, respectively. Considering the displacement between the upper and the lower layers, there should exist q_z modulation for the MEs. Taking this into account, we can get the spectra of the MEs through $\mathcal{X}''(q, q_z, \omega) = \mathcal{X}_S''(q, \omega) + \mathcal{X}_D''(q, \omega) \cos q_z$, here in this paper we have set the displacement between the upper and the lower layers to be the unit length.

For simplicity, the rigid band approximation is used to study the doping evolution behaviors of the normal state MEs of the nickelate $\text{La}_3\text{Ni}_2\text{O}_7$. Throughout the paper, T is set to be 0.001 and $J = U/4$ is assumed. The energies are all in unit of eV. All the calculations are carried out for a 256×256 lattice.

III. THE NUMERICAL RESULTS

A. Magnetic excitations for the system with $n = 3.0$

The low energy MEs are tightly related to the topology of the Fermi surfaces. In panel (a) of Fig. 1, we show the momentum distribution of the low energy electronic states within an energy window of 0.08 eV around the Fermi energy and their dominated orbital components. The electron α and hole β pockets are centered at $(0,0)$ and (π, π) in the Brillouin zone, respectively. They are mainly composed of the $3d_{x^2-y^2}$ orbital, especially around the diagonal region of the Fermi surfaces. In contrast, the hole γ pocket centered at (π, π) are fully dominated by the $3d_{z^2}$ orbital. Meanwhile, it can be seen from panel (a) that the γ pocket is much thicker than the α and β ones, which indicates that it has larger density of states (DOS) around the Fermi level, partially due to its approach to the band edge.

In panel (b) of Fig. 1, we show the momentum dependence of the MEs for $U = 1.1$, $\omega = 0.02$ and $q_z = 0$. The MEs show ferromagnetic (FM) correlations as indicated by the four peaks around $(0,0)$. By decomposition of the spin susceptibility into the orbital channels, it can be confirmed that these

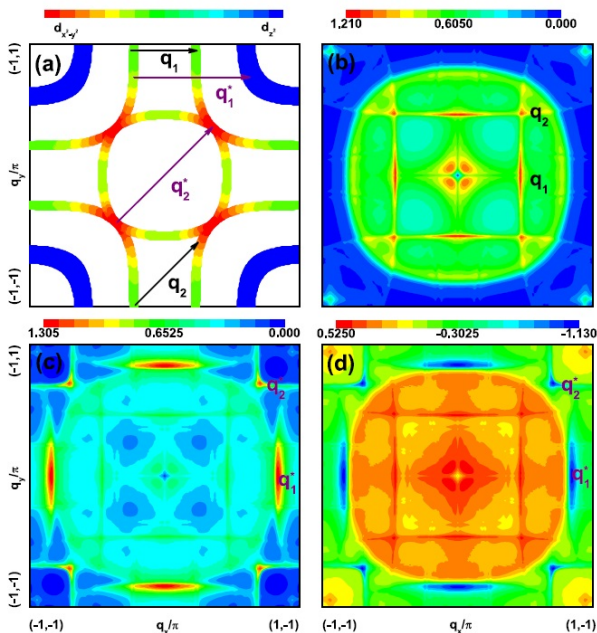


FIG. 1. (Color online) Panel (a) is the Fermi surfaces and its orbital compositions for $n = 3.0$. (b), (c) and (d) are the momentum distribution of the total, intralayer and interlayer magnetic spectra, respectively. The corresponding parameters are $U = 1.1$, $\omega = 0.02$, and $q_z = 0$.

FM MEs arise mainly from the $3d_{z^2}$ orbital. The contribution of the $3d_{x^2-y^2}$ orbital to these FM correlations are negligibly small. It was further found that these FM modes will be suppressed with the increasing of U . Away from $(0,0)$, there exist four peaks denoted by q_2 which reside along the diagonal direction and form the corners of a square. On the four edges of the square, other modes emerge with the characteristic momentum q_1 , as shown in Fig. 1 (b). As indicated by the black arrows in Fig. 1 (a), both the q_1 and q_2 modes are attributed to the particle-hole scatterings of the β band, due to the well-nested straight segments of the β pocket around $(0, \pm\pi)$ and $(\pm\pi, 0)$. This square-like pattern had been established by previous theoretical studies [7, 14], although where only the real part of the zero energy spin susceptibility was concerned. To reveal the possible interlayer modulations of the MEs, we calculated the intralayer and the interlayer magnetic spectra of χ_S'' and χ_D'' , respectively. The results are shown in panels (c) and (d) of Fig. 1, correspondingly. Clearly, the square-like pattern remains for both the intralayer and the interlayer MEs. However, the most prominent features are four additional peaks around (π, π) and four rod-like structure around $(\pm\pi, 0)$ and $(0, \pm\pi)$, which are denoted as q_2^* and q_1^* , respectively. As shown in Fig. 1 (c) and (d), comparing to that of the square-like pattern, these new MEs show significantly larger intensity. Most importantly, both the q_1^* and q_2^* modes show anti-phase relation between the intralayer and the interlayer spin susceptibility, which reflects the fact that there exists strong interlayer antiferromagnetic correlations. Thus, it can be expected that the MEs will exhibit strong q_z dependence.

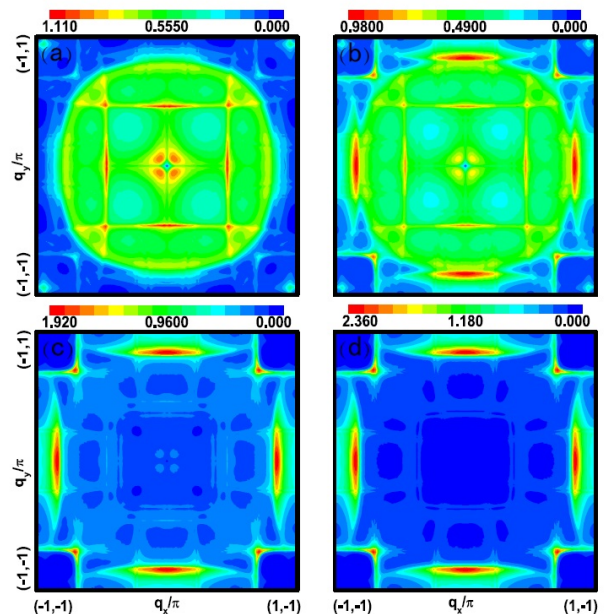


FIG. 2. (Color online) q_z evolution of the MEs for $U = 1.1$, $\omega = 0.02$. Panels (a), (b), (c) and (d) are the MEs for $q_z = 0.2\pi$, 0.4π , 0.7π and π , respectively.

In Fig. 2, for illustration, we show this q_z evolution of the MEs for $U = 1.1$ and $\omega = 0.02$. Their patterns for $q_z = 0.2\pi$, 0.4π , 0.7π and π are shown in panels (a), (b), (c) and (d), respectively. Clearly, with the increasing of q_z , the structure of the MEs change dramatically. For small q_z , the MEs are still dominated by the square-like pattern which arises from the intraband particle-hole excitations of the β pocket. When q_z increases to be around 0.4π , two new q_1^* and q_2^* modes emerge, and they coexist with the original q_1 and q_2 modes. With further increasing of q_z , the q_1 and q_2 modes decrease in intensity gradually, and they disappear in the large q_z regime. The resultant MEs are fully dominated by the q_1^* and q_2^* modes, as depicted in panels (c) and (d) of Fig. 2. In contrast to the MEs with small q_z , where the dominate features are attributed to the intraband particle-hole excitations. For large q_z , they turn to be dominated by the interband particle-hole excitations. Specifically, the q_1^* mode arises from the particle-hole excitations between the β and the γ pockets, while the q_2^* mode mainly originates from the particle-hole scatterings between the β and the α pockets. The typical scattering processes are shown in panel (a) of Fig. 1. The above mentioned hidden q_z dependent structures of the MEs had not been revealed by the previous studies [7, 14]. It is interesting to notice that the MEs pattern for large q_z near π shares quite similar structure with that of the previously established SDW interaction $V_{SDW}(q)$ which was proposed to be responsible for the emergence of superconductivity [26]. Here, we identify that the q_1^* and q_2^* modes are associated with the interlayer antiferromagnetic correlations. They shall play an important role if the magnetic fluctuation is regarded as the pairing glue.

Now we turn to the energy evolution of the MEs. The typical patterns of the MEs are shown in Fig. 3 for $\omega = 0.06$,

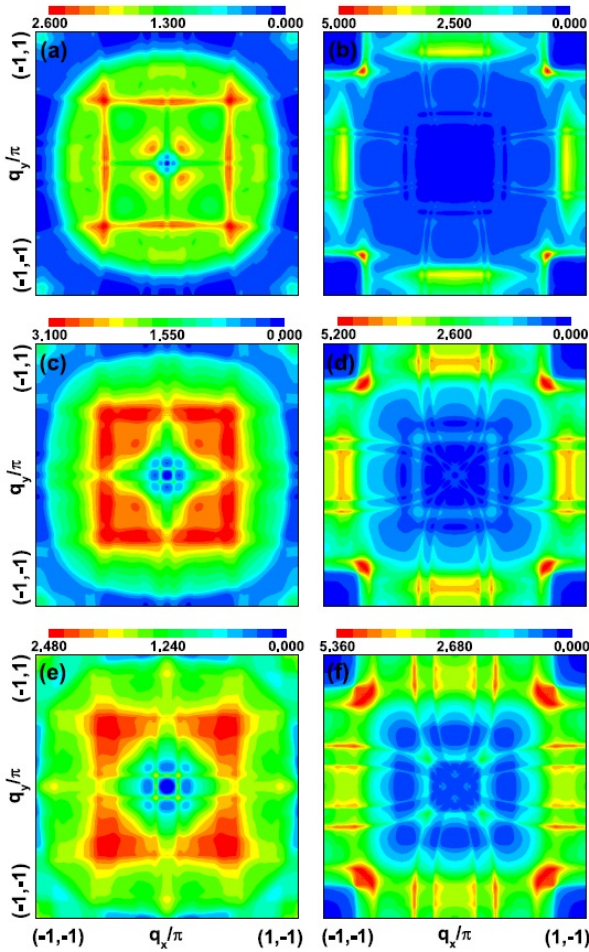


FIG. 3. (Color online) Energy evolution of the MEs. Panels (a) and (b) are the MEs for $q_z = 0$ and $q_z = \pi$, respectively, at a given energy of $\omega = 0.06$. Panels (c), (d) and (e), (f) are the same with (a), (b) but for $\omega = 0.12$ and 0.2 , respectively.

0.12 and 0.2. For small q_z , with the increasing of energy, each of the q_1 modes splits into two parts which move gradually toward the location of the q_2 modes and finally merge with them in the high energy regime, giving rise to the significantly broadened peaks in momentum space. Generally, the broadening of the peaks of the MEs can be expected due to the much more available particle-hole pairs when the energy becomes large. For large q_z near π , the q_2^* modes persist up to the high energy regime. Also, their peaks broaden steadily with the increasing of energy. In contrast, as shown in panels (d) and (f) of Fig. 3, the q_1^* modes split gradually into multiple peaks. This splitting of the q_1 and q_1^* modes with energy can be understood by analyzing the nesting behaviors of the corresponding constant energy contours (CECs). But here we only focus on the main features of the MEs.

To further reveal the q_z evolution of the MEs. In Fig. 4, we show their energy dependence along the high symmetry direction for various q_z . As depicted in panel (a) of Fig. 4, for small q_z near 0, the MEs are dominated by the q_1 and q_2 modes which persist up to the high energy regime. With the

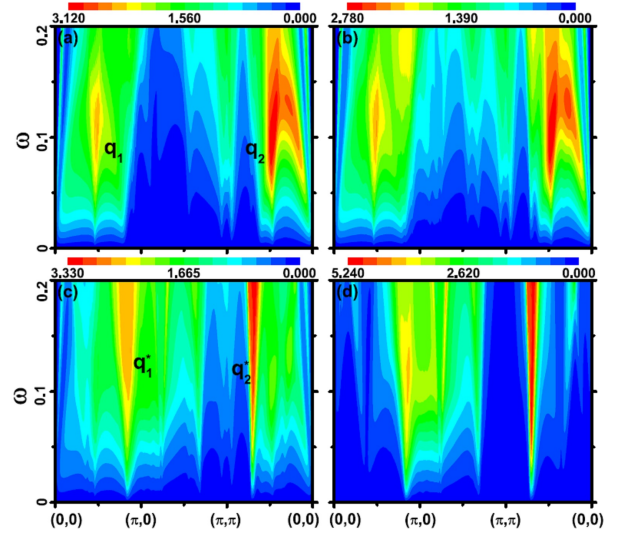


FIG. 4. (Color online) The $q - \omega$ dependence of the MEs along the high symmetry direction. Panels (a), (b), (c) and (d) are for $q_z = 0, \pi/4, \pi/2$ and π , respectively.

increasing of q_z , the intensity of the q_1 and q_2 modes diminish gradually. Meanwhile, the q_1^* and q_2^* modes emerge with their intensity increasing steadily. They rule the behaviors of the MEs for large q_z . As shown in Fig. 3 and 4, the MEs patterns of the nickelate $\text{La}_3\text{Ni}_2\text{O}_7$ change little with the increasing of energy. This is in sharp contrast with those of the copper-oxide [43, 46] and iron-based superconductors [54] where the structure transition of the MEs with energy usually happens. For cuprates in which the Van Hove singularity plays the crucial role in the behaviors of the MEs, the associated CECs move toward or away from the antinodal region with the variation of energy. Thus, a structure transition of the MEs with energy is usually expected [43, 46]. While for iron-based superconductors, both the electron and the hole pockets are generally small in size. As a result, the shape of the CECs change significantly with energy, giving rise to the structure transition of the MEs [54]. Here, we emphasize that the CECs of the energy bands of $\text{La}_3\text{Ni}_2\text{O}_7$ change little with energy, especially for those of the α and the β pockets due to the fact that they are large in both the size and the Fermi velocity. As a result, the patterns of the MEs can persist up to the high energy regime.

B. Doping behaviors of the magnetic excitations around $n = 3.0$

In the previous section, we discussed the normal state MEs with the filling number of $n = 3.0$ which seems to be related to the moderately pressurized nickelate $\text{La}_3\text{Ni}_2\text{O}_7$ which exhibits a superconducting transition temperature of about 80 K. It is interesting to know the doping evolution behaviors of the MEs because the topology of the Fermi surfaces may change prominently with carrier doping. In Fig. 5, we plotted the typical Fermi surfaces and their orbital compositions for the

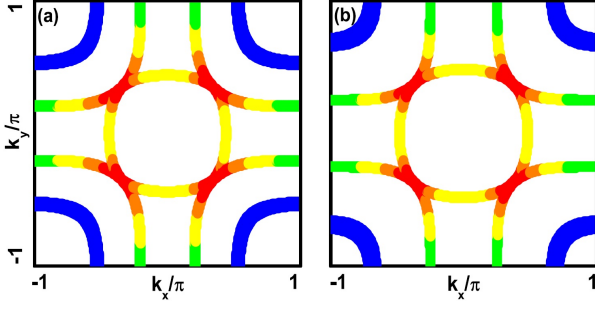


FIG. 5. (Color online) The Fermi surfaces and their orbital compositions. Panels (a) and (b) are for $n = 2.8$ and 3.2 , respectively.

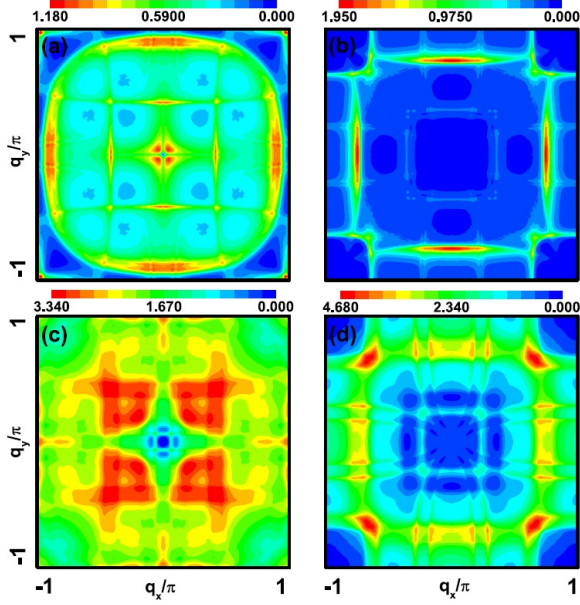


FIG. 6. (Color online) The MEs for the hole-doped system with $n = 2.8$. Panels (a) and (b) are for $\omega = 0.02$ but with $q_z = 0$ and $q_z = \pi$, respectively. Panels (c) and (d) are the same with (a) and (b) but for $\omega = 0.14$.

hole-doped system of $n = 2.8$ and the electron-doped one of $n = 3.2$. Comparing to Fig. 1 (a), it can be seen that the α pocket shrinks with the decreasing of the filling number n . In contrast, the β and γ pockets expand steadily. Expect these, the topology of the Fermi surfaces keeps unchanged comparing to the case of $n = 3.0$.

In Fig. 6, we show the patterns of the MEs for the hole-doped system with $n = 2.8$. As indicated by Fig. 6 (a), the square-like MEs composed by the q_1 and q_2 modes and the FM correlations remain at a low energy of $\omega = 0.02$ for $q_z = 0$. In addition, new MEs develop near $(0, \pm\pi)$ and $(\pm\pi, 0)$ with sizable intensity. Actually, as shown in Fig. 1 (b), these MEs have already show up for $n = 3.0$ where their intensity is weaker than that of the q_1 and q_2 modes. These MEs should be attributed to the particle-hole scatterings within the γ pocket. It has been carefully checked that these modes move gradually toward $(0, \pm\pi)$ and $(\pm\pi, 0)$ with the decreasing of the

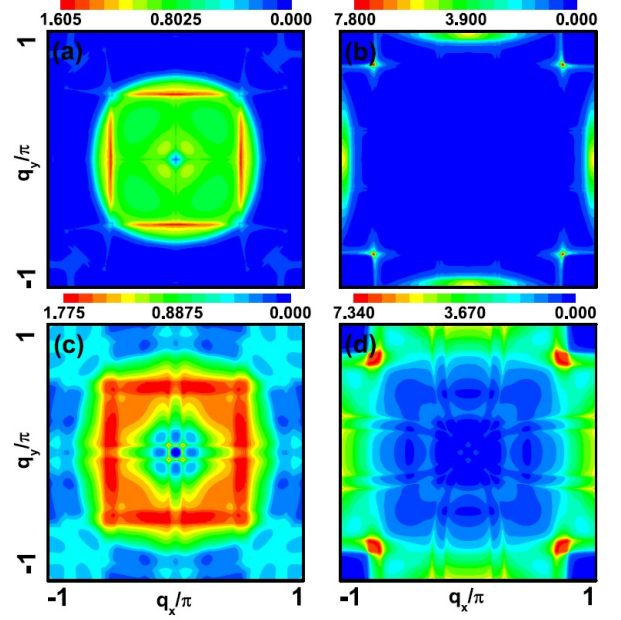


FIG. 7. (Color online) The MEs for the electron-doped system with $n = 3.2$. Panels (a) and (b) are for $\omega = 0.02$ but with $q_z = 0$ and $q_z = \pi$, respectively. Panels (c) and (d) are the same with (a) and (b) but for $\omega = 0.14$.

filling number. This coincides basically with the expansion of the γ pocket with hole-doping. Together with the q_1 and q_2 modes, these MEs for small q_z are all dominated by the intraband particle-hole excitations mainly from the γ and the β pockets, respectively. With the increasing of q_z , all these modes diminish gradually. Finally, the MEs are fully dominated by the q_1^* and q_2^* modes in the large q_z regime, just like the $n = 3.0$ case. It is interesting to notice that the q_1^* modes move away from the $(0, \pm\pi)$ and $(\pm\pi, 0)$ region. This is due to the fact that both the hole β and γ pockets expand in size with the decreasing of the filling number. Naturally, the length of q_1^* decreases because it connects the β pocket with the γ one (see Fig. 1 (a)). This further confirms that the q_1^* modes originate from the particle-hole scatterings between the β and the γ pockets. In contrast, the q_2^* modes move rather slowly with hole-doping due to the much larger Fermi velocity of the α and β bands comparing to that of the γ one. The energy evolution behaviors of the MEs are quite similar to those presented in Fig. 3 for $n = 3.0$. With the increasing of energy, as shown in Fig. 6 (c) for $\omega = 0.14$, the typical MEs for small q_z turn gradually to be dominated by the broad peaks around q_2 . Furthermore, the q_z evolutions of the MEs are also analogous to those of the $n = 3.0$ case. Specifically, the q_2^* and the splitted q_1^* modes show up with prominent intensity for large q_z around π . We have carefully checked that the above features of the MEs do not show qualitative changes up to the heavily hole-doped region around $n = 2.6$.

For the electron-doped case, as shown in Fig. 7, the main features of the MEs remain for large q_z . They are also dominated by the q_1^* and q_2^* modes. Due to the contraction of the β and the γ pockets with electron-doping, the q_1^* modes move

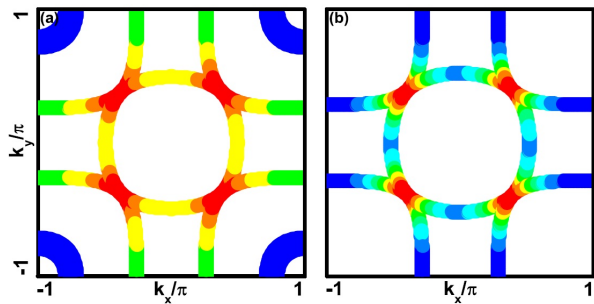


FIG. 8. (Color online) The Fermi surfaces and their orbital compositions for $n = 3.3$ (a) and 3.5 (b), respectively.

toward the $(0, \pm\pi)$ and $(\pm\pi, 0)$ region, contrary to that of the hole-doped case. And they reside just at $(0, \pm\pi)$ and $(\pm\pi, 0)$ for $n = 3.2$. Comparing to the hole-doped scenario, the low energy MEs near $(0, \pm\pi)$ and $(\pm\pi, 0)$ disappear for small q_z , as shown in Fig. 7 (a) for $q_z = 0$. This is due to the fact that the hole γ pocket shrinks and changes its shape from square to circle gradually with electron-doping. Thus, the original well-nesting property of the γ pocket diminishes gradually, leading to the absence of the modes associated with the particle-hole excitations within the γ pocket.

C. Distinct MEs across the Lifshitz transition

With further increasing of electron-doping, the γ pocket will turn gradually to be under the Fermi level, i.e., a Lifshitz transition will occur. This change of the Fermi surfaces topology is shown in Fig. 8. For the filling of $n = 3.3$ above the Lifshitz transition, the hole γ pocket coexists with the electron α and the hole β ones. But when n increases to be 3.5 , the γ pocket disappears. Meanwhile, the orbital compositions of the α and the β pockets change significantly around the Fermi level. In contrast to that above the Lifshitz transition where they are dominated by the $3d_{x^2-y^2}$ orbital. Below the transition, both pockets have prominent $3d_{z^2}$ orbital weight, especially around the $(\pm\pi, 0)$ and $(0, \pm\pi)$ region. By studying the doping evolutions of the Fermi surfaces, it can be confirmed that the Lifshitz transition occurs around $n = 3.4$.

Now we turn to the study of the MEs across the Lifshitz transition. For illustration, the typical MEs are shown in Fig. 9 for $n = 3.3$ and 3.5 above and below the Lifshitz transition, respectively. For $n = 3.3$, it can be seen from Fig. 9 (a) that the q_1 and q_2 modes remain for $\omega = 0.06$ and $q_z = 0$, although the q_2 modes are rather weak in intensity. However, the most prominent feature of the MEs is a ring-like structure centered at $(0, 0)$. This is fully attributed to the particle-hole scatterings within the small circular-shaped γ pocket. Similar pattern of the MEs had been obtained for the monolayer cuprates [55]. Thus, this kind of pattern can be seen as a hallmark of the MEs near the Lifshitz transition. With the increasing of q_z , the patterns of the MEs turn gradually to be dominated by the familiar q_1^* and q_2^* modes as usual. The typical MEs are shown in Fig. 9 (b), they are nearly the same with those for

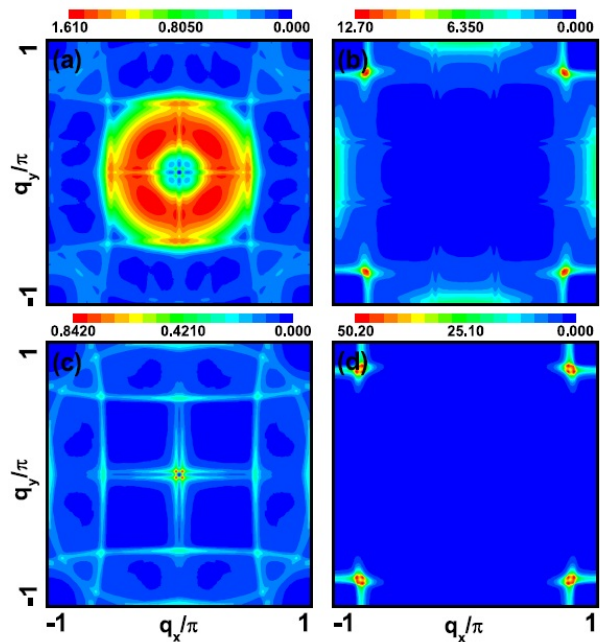


FIG. 9. (Color online) The MEs across the Lifshitz transition around $n = 3.4$. Panels (a) and (b) are the MEs for $n = 3.3$, $\omega = 0.06$ but with $q_z = 0$ and $q_z = \pi$, respectively. Panels (c) and (d) are the same with (a) and (b) but for $n = 3.5$.

$n = 3.0$. Below the Lifshitz transition, the square-like MEs formed by the q_1 and q_2 modes remain for small q_z . This is due to the fact that these modes originate from the particle-hole scatterings between the flat segments of the β pocket which changes little with electron-doping. In addition, as depicted in panel (c) of Fig. 9, the FM modes emerge near $(0, 0)$. They should be attributed to the particle-hole scatterings between the α and the β pockets around their touch points in the Brillouin zone. We have checked that these FM modes move away from $(0, 0)$ gradually with the increasing of energy due to the splitting between the CECs of the α and the β pockets. With the increasing of q_z , the patterns of the MEs change dramatically. For large q_z around π , the q_1^* modes disappear totally due to the absence of the γ pocket, and the resultant MEs are fully dominated by the q_2^* modes with rather high intensity which indicates a strong tendency toward the SDW order. It should be noticed that, for this SDW order, the in-plane spins tend to form an incommensurate order with momentum q_2^* near (π, π) , while they prefer to align antiferromagnetically between the upper and the lower nickel-oxygen layers.

Actually, we have performed the detailed numerical calculations of the MEs for the wide doping region from $n = 3.4$ to $n = 4.0$. We find that the above mentioned features of the MEs are very robust below the Lifshitz transition. Both the square-like pattern of the MEs for small q_z and the q_2^* modes for large q_z persist up to the high energy regime. Furthermore, all these behaviors of the MEs remain in the wide doping region from $n = 3.5$ to $n = 4.0$. Moreover, the intensity of q_2^* modes overwhelms that with small q_z in this doping region. And it grows rapidly with electron-doping which sig-

nals the strong tendency toward the magnetic order. This is in sharp contrast with the MEs above the Lifshitz transition where intensities of the small q_z modes are usually comparable to those with large q_z . The strong tendency toward the SDW order can be understood in the following way. Below the Lifshitz transition, the γ band is fully occupied with the electron number $n_\gamma = 2$. For a filling of $n = 4$, the size of the electron α and the hole β pockets should be equal to fulfill $n_\alpha + n_\beta = 2$. Considering the square-like shape of the Fermi surfaces, there should exist perfect nesting between the electron α and the hole β pockets, just like what happened in the iron-based superconductors [56]. Thus, one can expect that the pressurized $\text{La}_3\text{Ni}_2\text{O}_7$ shall be in the SDW phase which ordered at (π, π, π) around the filling of $n = 4$. In this way, it seems that the superconducting phase is in close proximity to the SDW state and it can emerge through hole-doping to the "parental compound" of the pressurized nickelates with $n = 4$. From this point of view, the pressurized nickel-based superconductors seem to share some common features with their iron-based counterparts.

IV. SUMMARY AND CONCLUSIONS

In summary, we have studied the normal state behaviors of the MEs in the double-layer pressurized nickelate $\text{La}_3\text{Ni}_2\text{O}_7$ based on a realistic theoretical model [7]. For $n = 3.0$ which seems to be most relevant to the material which realizes the high temperature superconductivity of about 80 K under the moderate pressure above 14 GPa. It was found that the MEs have very strong interlayer modulations by q_z due to the displacement between the upper and the lower nickel-oxygen layers. For small q_z , the low energy MEs are dominated by a square-like structure composed of the q_1 and q_2 modes which both originate from the intraband particle-hole scatterings of the β pocket. The square-shaped patterns of the MEs persist with the increasing of energy, but they turn to be four broad peaks around $(\pm\pi/2, \pm\pi/2)$ in the high energy regime. The pattern of the MEs changes dramatically when q_z becomes large. Especially, the square pattern of the MEs for small q_z disappears gradually with the increasing of q_z . Finally, for large q_z around π , the MEs are dominated by the q_1^* modes which locate around $(\pm\pi, 0)$ and $(0, \pm\pi)$ and the q_2^* modes around (π, π) . To our knowledge, these hidden q_z dependent structures of the MEs had not been established by previous studies [7, 14]. It was carefully checked that the q_1^* modes originate from the particle-hole scatterings between the β and the γ pockets. While the q_2^* modes mainly arise from the particle-hole excitations between the β and the α pockets, and they split gradually into parts in the high energy regime. Generally, the MEs show significantly larger intensity for the modes with q_z near π . Thus, these interlayer antiferromagnetic modes are expected to play a prominent role in the formation of Cooper pairs. Actually, the patterns of the MEs found here for large q_z are very similar to the momentum structure of the SDW interaction established before which was proposed to be the pairing glue [26].

With hole-doping, both the square pattern of the MEs for

small q_z and the q_1^* and q_2^* modes for large q_z persist up to the heavily hole-doping regime around $n = 2.6$, although new MEs will emerge near the boundary of the Brillouin zone attributing to the particle-hole scatterings within the γ pocket which turns to be the square-like shape with the gradually increasing of hole-doping. On the other hand, for electron-doping up to $n = 3.3$, the patterns of the MEs and their energy and q_z dependence are qualitatively the same with those for $n = 3.0$. Thus, the MEs exhibit very robust features in both the hole- and electron-doping region around $n = 3.0$.

With further increasing of electron-doping, the γ pocket turns gradually to be under the Fermi level, i.e., a Lifshitz transition will occur around $n = 3.4$. Consequently, the behaviors of the MEs change dramatically. Just above the transition, the MEs for small q_z turn to be dominated by a ring-like structure centered at $(0, 0)$ instead of the square-like pattern far above the transition point. These ring-like MEs should be attributed to the particle-hole scatterings within the γ pocket. Such behavior of the MEs had been established for the monolayer cuprates before [55]. Thus, it seems to be a hallmark of the low energy MEs near the Lifshitz transition. In contrast, the MEs for large q_z are still dominated by the q_1^* and q_2^* modes, although the intensity of the q_1^* modes weakens significantly. Below the transition, the behaviors of the MEs change dramatically. The most prominent features of the MEs for large q_z are the absence of the q_1^* modes and the strongly enhanced intensity of the q_2^* modes. In contrast, the MEs with small q_z keep to be the square-like pattern but with much weakened intensity. As a result, the MEs are fully ruled by the q_2^* modes which indicate the strong tendency toward the SDW order.

It is interesting to notice that the μSR [36, 37], NMR [38] and RIXS [35] measurements on the double-layer nickelates had confirmed the development of the SDW order at ambient pressure. Furthermore, it was found that the SDW ordered at $(\pi/2, \pi/2, \pi)$. Thus, the superconductivity is in close proximity with the SDW state in the pressure-temperature phase diagram. However, here we investigate the doping evolution behaviors of the MEs of the double-layer nickelate $\text{La}_3\text{Ni}_2\text{O}_7$ with fixed moderate pressure at which superconductivity emerges. We predict the existence of a SDW phase which orders around (π, π, π) for the heavily electron-doped material under moderate pressures. This SDW instability is governed by the perfect nesting between the α and the β pockets at $n = 4.0$. Due to the fact that the spin susceptibility will be further enhanced by interaction, the SDW state may develop around $n = 3.5$, i.e., the doping level of about 0.25 electron per Ni-site, according to our numerical results. If this is true, it seems that superconductivity emerges through hole-doping to the "parental compound" of the pressurized nickelates with $n = 4.0$. In this way, the nickel-based superconductors share very similar features with their iron-based counterparts. We expect the doping-temperature phase diagram of the pressurized $\text{La}_3\text{Ni}_2\text{O}_7$ will be explored experimentally and theoretically in the near future.

V. ACKNOWLEDGMENTS

This work was supported by the National Natural Science Foundation of China (Grants Nos. 11804290, 11647072).

-
- [1] H. Sun, M. Huo, X. Hu, J. Li, Z. Liu, Y. Han, L. Tang, Z. Mao, P. Yang, B. Wang, J. Cheng, D.-X. Yao, G.-M. Zhang, and M. Wang, Signatures of superconductivity near 80 K in a nickelate under high pressure, *Nature* **621**, 493 (2023).
- [2] Y. Zhang, D. Su, Y. Huang, Z. Shan, H. Sun, M. Huo, K. Ye, J. Zhang, Z. Yang, Y. Xu, Y. Su, R. Li, M. Smidman, M. Wang, L. Jiao, and H. Yuan, High-temperature superconductivity with zero resistance and strange-metal behaviour in $\text{La}_3\text{Ni}_2\text{O}_7 - \delta$, *Nature Physics*, (2024).
- [3] J. Hou, P.-T. Yang, Z.-Y. Liu, J.-Y. Li, P.-F. Shan, L. Ma, G. Wang, N.-N. Wang, H.-Z. Guo, J.-P. Sun, Y. Uwatoko, M. Wang, G.-M. Zhang, B.-S. Wang, and J.-G. Cheng, Emergence of high-temperature superconducting phase in pressurized $\text{La}_3\text{Ni}_2\text{O}_7$ crystals, *Chinese Physics Letters* **40**, 117302 (2023).
- [4] Y. Zhou, J. Guo, S. Cai, H. Sun, P. Wang, J. Zhao, J. Han, X. Chen, Y. Chen, Q. Wu, Y. Ding, T. Xiang, H. kwang Mao, and L. Sun, *Investigations of key issues on the reproducibility of high- T_c superconductivity emerging from compressed $\text{La}_3\text{Ni}_2\text{O}_7$* (2024), arXiv:2311.12361 [cond-mat.supr-con].
- [5] J. Li, P. Ma, H. Zhang, X. Huang, C. Huang, M. Huo, D. Hu, Z. Dong, C. He, J. Liao, X. Chen, T. Xie, H. Sun, and M. Wang, *Pressure-driven right-triangle shape superconductivity in bilayer nickelate $\text{La}_3\text{Ni}_2\text{O}_7$* (2024), arXiv:2404.11369 [cond-mat.supr-con].
- [6] G. Wang, N. N. Wang, X. L. Shen, J. Hou, L. Ma, L. F. Shi, Z. A. Ren, Y. D. Gu, H. M. Ma, P. T. Yang, Z. Y. Liu, H. Z. Guo, J. P. Sun, G. M. Zhang, S. Calder, J.-Q. Yan, B. S. Wang, Y. Uwatoko, and J.-G. Cheng, Pressure-induced superconductivity in polycrystalline $\text{La}_3\text{Ni}_2\text{O}_{7-\delta}$, *Phys. Rev. X* **14**, 011040 (2024).
- [7] Z. Luo, X. Hu, M. Wang, W. Wú, and D.-X. Yao, Bilayer two-orbital model of $\text{La}_3\text{Ni}_2\text{O}_7$ under pressure, *Phys. Rev. Lett.* **131**, 126001 (2023).
- [8] X.-Z. Qu, D.-W. Qu, J. Chen, C. Wu, F. Yang, W. Li, and G. Su, Bilayer $t-J-J_\perp$ model and magnetically mediated pairing in the pressurized nickelate $\text{La}_3\text{Ni}_2\text{O}_7$, *Phys. Rev. Lett.* **132**, 036502 (2024).
- [9] G. Heier, K. Park, and S. Y. Savrasov, Competing d_{xy} and s_\pm pairing symmetries in superconducting $\text{La}_3\text{Ni}_2\text{O}_7$: LDA + FLEX calculations, *Phys. Rev. B* **109**, 104508 (2024).
- [10] Y.-H. Tian, Y. Chen, J.-M. Wang, R.-Q. He, and Z.-Y. Lu, Correlation effects and concomitant two-orbital s_\pm -wave superconductivity in $\text{La}_3\text{Ni}_2\text{O}_7$ under high pressure, *Phys. Rev. B* **109**, 165154 (2024).
- [11] Z. Pan, C. Lu, F. Yang, and C. Wu, Effect of rare-earth element substitution in superconducting $\text{La}_3\text{Ni}_2\text{O}_7$ under pressure, arXiv preprint arXiv:2309.06173 <https://doi.org/10.48550/arXiv.2309.06173> (2023).
- [12] Y. Shen, M. Qin, and G.-M. Zhang, Effective bi-layer model hamiltonian and density-matrix renormalization group study for the high- T_c superconductivity in $\text{La}_3\text{Ni}_2\text{O}_7$ under high pressure, *Chinese Physics Letters* **40**, 127401 (2023).
- [13] Z. Liu, M. Huo, J. Li, Q. Li, Y. Liu, Y. Dai, X. Zhou, J. Hao, Y. Lu, M. Wang, and H.-H. Wen, *Electronic correlations and partial gap in the bilayer nickelate $\text{La}_3\text{Ni}_2\text{O}_7$* (2024), arXiv:2307.02950 [cond-mat.supr-con].
- [14] F. Lechermann, J. Gondolf, S. Bötzel, and I. M. Eremin, Electronic correlations and superconducting instability in $\text{La}_3\text{Ni}_2\text{O}_7$ under high pressure, *Phys. Rev. B* **108**, L201121 (2023).
- [15] Y. Wang, K. Jiang, Z. Wang, F.-C. Zhang, and J. Hu, *Electronic structure and superconductivity in bilayer $\text{La}_3\text{Ni}_2\text{O}_7$* (2024), arXiv:2401.15097 [cond-mat.supr-con].
- [16] Y. Zhang, L.-F. Lin, A. Moreo, T. A. Maier, and E. Dagotto, Electronic structure, magnetic correlations, and superconducting pairing in the reduced ruddlesden-popper bilayer $\text{La}_3\text{Ni}_2\text{O}_6$ under pressure: Different role of $d_{3z^2-r^2}$ orbital compared with $\text{La}_3\text{Ni}_2\text{O}_7$, *Phys. Rev. B* **109**, 045151 (2024).
- [17] H. Lange, L. Homeier, E. Demler, U. Schollwöck, F. Grusdt, and A. Bohrdt, Feshbach resonance in a strongly repulsive ladder of mixed dimensionality: A possible scenario for bilayer nickelate superconductors, *Phys. Rev. B* **109**, 045127 (2024).
- [18] Q. Qin and Y.-f. Yang, High- T_c superconductivity by mobilizing local spin singlets and possible route to higher T_c in pressurized $\text{La}_3\text{Ni}_2\text{O}_7$, *Phys. Rev. B* **108**, L140504 (2023).
- [19] Z. Luo, B. Lv, M. Wang, W. Wú, and D.-X. Yao, *High- T_c superconductivity in $\text{La}_3\text{Ni}_2\text{O}_7$ based on the bilayer two-orbital t-j model* (2023), arXiv:2308.16564 [cond-mat.supr-con].
- [20] K. Jiang, Z. Wang, and F.-C. Zhang, High-temperature superconductivity in $\text{La}_3\text{Ni}_2\text{O}_7$, *Chinese Physics Letters* **41**, 017402 (2024).
- [21] J. Huang, Z. D. Wang, and T. Zhou, Impurity and vortex states in the bilayer high-temperature superconductor $\text{La}_3\text{Ni}_2\text{O}_7$, *Phys. Rev. B* **108**, 174501 (2023).
- [22] Y.-f. Yang, G.-M. Zhang, and F.-C. Zhang, Interlayer valence bonds and two-component theory for high- T_c superconductivity of $\text{La}_3\text{Ni}_2\text{O}_7$ under pressure, *Phys. Rev. B* **108**, L201108 (2023).
- [23] C. Lu, Z. Pan, F. Yang, and C. Wu, Interlayer-coupling-driven high-temperature superconductivity in $\text{La}_3\text{Ni}_2\text{O}_7$ under pressure, *Phys. Rev. Lett.* **132**, 146002 (2024).
- [24] C. Lu, Z. Pan, F. Yang, and C. Wu, *Interplay of two e_g orbitals in superconducting $\text{La}_3\text{Ni}_2\text{O}_7$ under pressure* (2023), arXiv:2310.02915 [cond-mat.supr-con].
- [25] J.-R. Xue and F. Wang, Magnetism and superconductivity in the t-J model of $\text{La}_3\text{Ni}_2\text{O}_7$ under multiband gutzwiller approximation, *Chinese Physics Letters* **41**, 057403 (2024).
- [26] Q.-G. Yang, D. Wang, and Q.-H. Wang, Possible s_\pm -wave superconductivity in $\text{La}_3\text{Ni}_2\text{O}_7$, *Phys. Rev. B* **108**, L140505 (2023).
- [27] J.-X. Zhang, H.-K. Zhang, Y.-Z. You, and Z.-Y. Weng, *Strong pairing originated from an emergent Z_2 berry phase in $\text{La}_3\text{Ni}_2\text{O}_7$* (2023), arXiv:2309.05726 [cond-mat.str-el].
- [28] Y. Zhang, L.-F. Lin, A. Moreo, T. A. Maier, and E. Dagotto, Structural phase transition, s_\pm -wave pairing, and magnetic stripe order in bilayered superconductor $\text{La}_3\text{Ni}_2\text{O}_7$ under pressure, *Nature Communications* **15**, 2470 (2024).
- [29] Z. Fan, J.-F. Zhang, B. Zhan, D. Lv, X.-Y. Jiang, B. Normand, and T. Xiang, Superconductivity in nickelate and cuprate superconductors with strong bilayer coupling, *Phys. Rev. B* **110**, 024514 (2024).

- [30] Y. Zhang, L.-F. Lin, A. Moreo, T. A. Maier, and E. Dagotto, Trends in electronic structures and s_{\pm} -wave pairing for the rare-earth series in bilayer nickelate superconductor $R_3\text{Ni}_2\text{O}_7$, *Phys. Rev. B* **108**, 165141 (2023).
- [31] H. Oh and Y.-H. Zhang, Type-II $t-j$ model and shared superexchange coupling from Hund's rule in superconducting $\text{La}_3\text{Ni}_2\text{O}_7$, *Phys. Rev. B* **108**, 174511 (2023).
- [32] Y.-B. Liu, J.-W. Mei, F. Ye, W.-Q. Chen, and F. Yang, s^{\pm} -wave pairing and the destructive role of apical-oxygen deficiencies in $\text{La}_3\text{Ni}_2\text{O}_7$ under pressure, *Phys. Rev. Lett.* **131**, 236002 (2023).
- [33] J. Yang, H. Sun, X. Hu, Y. Xie, T. Miao, H. Luo, H. Chen, B. Liang, W. Zhu, G. Qu, C.-Q. Chen, M. Huo, Y. Huang, S. Zhang, F. Zhang, F. Yang, Z. Wang, Q. Peng, H. Mao, G. Liu, Z. Xu, T. Qian, D.-X. Yao, M. Wang, L. Zhao, and X. J. Zhou, Orbital-dependent electron correlation in double-layer nickelate $\text{La}_3\text{Ni}_2\text{O}_7$, *Nature Communications* **15**, 4373 (2024).
- [34] Y. Li, X. Du, Y. Cao, C. Pei, M. Zhang, K. Zhai, R. Xu, Z. Liu, Z. Li, J. Zhao, G. Li, Y. Qi, H. Guo, Y. Chen, and L. Yang, Electronic correlation and pseudogap-like behavior of high-temperature superconductor $\text{La}_3\text{Ni}_2\text{O}_7$, *Chin. Phys. Lett.* **41**, 087402 (2024).
- [35] X. Chen, J. Choi, Z. Jiang, J. Mei, K. Jiang, J. Li, S. Agrestini, M. Garcia-Fernandez, X. Huang, H. Sun, D. Shen, M. Wang, J. Hu, Y. Lu, K.-J. Zhou, and D. Feng, *Electronic and magnetic excitations in $\text{La}_3\text{Ni}_2\text{O}_7$* (2024), [arXiv:2401.12657](https://arxiv.org/abs/2401.12657) [cond-mat.supr-con].
- [36] K. Chen, X. Liu, J. Jiao, M. Zou, C. Jiang, X. Li, Y. Luo, Q. Wu, N. Zhang, Y. Guo, and L. Shu, Evidence of spin density waves in $\text{La}_3\text{Ni}_2\text{O}_{7-\delta}$, *Phys. Rev. Lett.* **132**, 256503 (2024).
- [37] R. Khasanov, T. J. Hicken, D. J. Gawryluk, L. P. Sorel, S. Bötzel, F. Lechermann, I. M. Eremin, H. Luetkens, and Z. Guguchia, *Pressure-induced split of the density wave transitions in $\text{La}_3\text{Ni}_2\text{O}_{7-\delta}$* (2024), [arXiv:2402.10485](https://arxiv.org/abs/2402.10485) [cond-mat.supr-con].
- [38] Z. Dan, Y. Zhou, M. Huo, Y. Wang, L. Nie, M. Wang, T. Wu, and X. Chen, *Spin-density-wave transition in double-layer nickelate $\text{La}_3\text{Ni}_2\text{O}_7$* (2024), [arXiv:2402.03952](https://arxiv.org/abs/2402.03952) [cond-mat.supr-con].
- [39] A. Damascelli, Z. Hussain, and Z.-X. Shen, Angle-resolved photoemission studies of the cuprate superconductors, *Rev. Mod. Phys.* **75**, 473 (2003).
- [40] C. Proust and L. Taillefer, The remarkable underlying ground states of cuprate superconductors, *Annual Review of Condensed Matter Physics* **10**, 409 (2019).
- [41] D. J. Scalapino, A common thread: The pairing interaction for unconventional superconductors, *Rev. Mod. Phys.* **84**, 1383 (2012).
- [42] H. J. Schulz, Incommensurate antiferromagnetism in the two-dimensional Hubbard model, *Phys. Rev. Lett.* **64**, 1445 (1990).
- [43] M. R. Norman, Linear response theory and the universal nature of the magnetic excitation spectrum of the cuprates, *Phys. Rev. B* **75**, 184514 (2007).
- [44] T. Das, R. S. Markiewicz, and A. Bansil, Reconstructing the bulk Fermi surface and superconducting gap properties from neutron scattering experiments, *Phys. Rev. B* **85**, 064510 (2012).
- [45] H. Y. Zhang, Y. Zhou, H. Q. Lin, and C. D. Gong, Commensurate magnetic excitations induced by band splitting and Fermi surface topology in n-type cuprates, *Journal of Physics: Condensed Matter* **25**, 155603 (2013).
- [46] H. Zhang, Y. Zhou, and C.-D. Gong, Non-d-wave superconductivity driven magnetic excitations features in underdoped cuprates, *Journal of the Physical Society of Japan* **82**, 094715 (2013), <https://doi.org/10.7566/JPSJ.82.094715>.
- [47] H. Yamase and H. Kohno, Magnetic excitation of t - J model with quasi-one-dimensional Fermi surface - possible relevance to LSCO systems, *Journal of the Physical Society of Japan* **70**, 2733 (2001), <https://doi.org/10.1143/JPSJ.70.2733>.
- [48] H. Yamase and W. Metzner, Magnetic excitations and their anisotropy in $\text{Yb}_2\text{Cu}_3\text{O}_{6+x}$: Slave-boson mean-field analysis of the bilayer t - j model, *Phys. Rev. B* **73**, 214517 (2006).
- [49] M. M. Korshunov and I. Eremin, Theory of magnetic excitations in iron-based layered superconductors, *Phys. Rev. B* **78**, 140509 (2008).
- [50] T. A. Maier and D. J. Scalapino, Theory of neutron scattering as a probe of the superconducting gap in the iron pnictides, *Phys. Rev. B* **78**, 020514 (2008).
- [51] T. A. Maier, S. Graser, D. J. Scalapino, and P. Hirschfeld, Neutron scattering resonance and the iron-pnictide superconducting gap, *Phys. Rev. B* **79**, 134520 (2009).
- [52] T. A. Maier, P. J. Hirschfeld, and D. J. Scalapino, Evolution of the neutron resonances in AFe_2Se_2 , *Phys. Rev. B* **86**, 094514 (2012).
- [53] M. Kovacic, M. H. Christensen, M. N. Gastiasoro, and B. M. Andersen, Spin excitations in the nematic phase and the metallic stripe spin-density wave phase of iron pnictides, *Phys. Rev. B* **91**, 064424 (2015).
- [54] A. Kreisel, S. Mukherjee, P. J. Hirschfeld, and B. M. Andersen, Spin excitations in a model of FeSe with orbital ordering, *Phys. Rev. B* **92**, 224515 (2015).
- [55] H.-Y. Zhang, X.-Q. Wu, F.-J. Kong, Y.-J. Bai, and N. Xu, Doping evolution of the magnetic excitations in the monolayer CuO_2 , *Journal of Physics: Condensed Matter* **32**, 415603 (2020).
- [56] I. I. Mazin, D. J. Singh, M. D. Johannes, and M. H. Du, Unconventional superconductivity with a sign reversal in the order parameter of $\text{LaFeAsO}_{1-x}\text{F}_x$, *Phys. Rev. Lett.* **101**, 057003 (2008).